Available online at www.sciencedirect.com
SCIENCE DIRECT
Journal of Photochemistry and Photobiology A: Chemistry 177 (2006) 43–54
Journal of Photochemistry and Photobiology A:Chemistry
www.elsevier.com/locate/jphotochem

Tuning the DNA binding modes of an anthracene derivative with salt

N.K. Modukuru, K.J. Snow, B. Scott Perrin Jr., A. Bhambhani, M. Duff, Challa V. Kumar *

Department of Chemistry, University of Connecticut, Storrs, CT 06269-3060, USA

Received 5 March 2005; received in revised form 21 April 2005; accepted 6 May 2005
Available online 21 June 2005

Abstract

The DNA binding properties of an anthracene derivative with substituents at the 9 and 10 positions, carrying four positive charges, are examined in calorimetric, spectroscopic and photocleavage studies. Isothermal titration calorimetric data indicated exothermic binding of the ligand to calf thymus DNA with a binding constant of $(1.4 \pm 0.5) \times 10^5\ M^{-1}$ and this value is much greater than binding of similar monocationic derivatives. The values for the other binding parameters were, $\Delta H = -3.5 \pm 0.4$ kcal/mol; $\Delta S = 11.6 \pm 1.6$ cal/mol K, and a binding site size of ~4 base pairs. Absorption spectral studies indicated small, but significant red shifts in the vibronic bands, and ~70% of hypochromism. The binding plots indicated bi-phasic binding of the ligand. At higher ionic strengths, the red shifts in the absorption spectra were abolished but significant hypochromism persisted.

Excitation and sensitized fluorescence spectral studies indicated weak energy transfer from the DNA bases to the ligand. Further more, energy transfer was reduced substantially at higher ionic strengths. Strong induced circular dichroism bands are noted, in the 300–400 nm region, and these are most likely dominated by the contributions from the groove bound form as well as the intercalated chromophore. Helix melting studies indicated improvement in the helix stability, and substantial increase in the melting temperature ($\Delta T_m > 17\ ^\circ C$). Differential scanning calorimetric data, on the other hand, indicated only minor improvements in the thermodynamic parameters. Irradiation of a mixture of the ligand (2 μM) and supercoiled pUC18 DNA (20 μM, @374 nm) resulted in the efficient formation of nicked circular DNA (>90%) in an hour. The data indicated at least two distinct binding modes, and one of these persisted at high ionic strengths (375 mM NaCl). Substitution at 9 and 10 positions of the anthracene ring system with positively charged residues resulted in multiple binding modes, and these are resolvable in ionic strength studies.

Keywords: Isothermal titration calorimetry; DSC; Photocleavage; DNA; Anthracene derivatives

1. Introduction

A clear understanding of the interaction of small molecules with DNA is important in the rational design of ligands that can bind to DNA with high affinity and selectivity [1]. Anthracene derivatives are among the many molecules that have been investigated for their binding to DNA, and some of these are promising chemotherapeutic agents. Pseudourea, for example, was one of the first anthracene derivatives to be tested in clinical trials, but it was withdrawn due to toxicity [2–4]. Anthracene itself was shown to be effective against certain skin ailments such as psoriasis [5]. Other anthracene derivatives that were tested for anticancer activity include ametantrone, mitoxantrone, and bisantrene [6]. These molecules are suggested to elicit their activity by binding to DNA [7], and the binding may involve groove/electrostatic as well as intercalative binding modes (Chart 1) [7].

One of our goals has been to investigate how substitutions at the 9 and 10 positions of the anthryl ring system influence the binding properties of the anthracene derivatives [8]. For example, 9-anthrylmethylammonium chloride (AMAC, Chart 2) provided one of the first examples to illustrate the intercalative binding of the anthryl nucleus [9]. The cationic side chain of AMAC enhances its solubility in aqueous media, and provides favorable electrostatic interactions with the helix. While the planar aromatic ring systems of the

* Corresponding author. Tel.: +1 860 486 3213.
E-mail address: Challa.Kumar@uconn.edu (C.V. Kumar).
URL: http://jasmin.chem.uconn.edu.

1010-6030/$ – see front matter © 2005 Elsevier B.V. All rights reserved.
doi:10.1016/j.jphotochem.2005.05.010

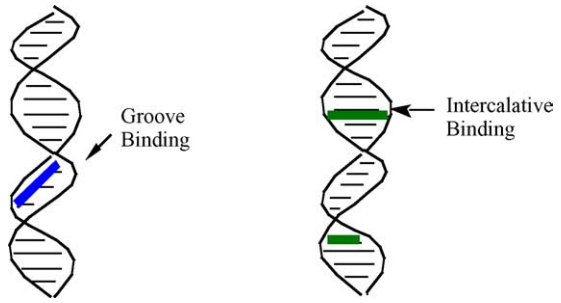

Chart 1. Two most common DNA binding modes for small molecules.

anthryl derivatives intercalate, the side chains are expected to lie in the DNA grooves [10,11].

Appropriate substituents at the 9 and 10 positions of the anthracene derivatives also influence the DNA binding properties such as binding modes, binding affinities, and binding specificity. For example, APAC (Chart 2) shows preference for AT-rich sites over GC-rich regions [9]. The steric, electrostatic, and geometric requirements of the substituents are expected to influence the favorable DNA binding modes of a given ligand [12]. Here, the influence of charge, and ionic strength on the binding properties of the anthryl ring system is tested using BEDA (Chart 2). BEDA has two side chains carrying a total of six CH_2 groups, and four cationic functions. Previous studies showed that BEDA has significant anticancer activity [13].

The cationic functions of BEDA are expected to promote the overall binding affinity via favorable electrostatic interactions with the negatively charged DNA helix, but they may also establish a significant barrier for intercalation. This is because one of the highly charged side chains will have to pass through the base stack (threading) for the complete intercalation of the anthryl chromophore. In this binding mode, the long axis of the anthracene nucleus will be aligned with the long axis of the base pair. Partial intercalation of the anthryl nucleus is possible, where the long axis of the anthracene ring system is oriented perpendicular to the long axis of the base pair, and this binding mode does not involve the threading of the helix by the cationic side chain. Alternatively, the multiple cationic charges of BEDA may stabilize groove binding, where the charged side chains may be aligned with the sugar-phosphate backbone.

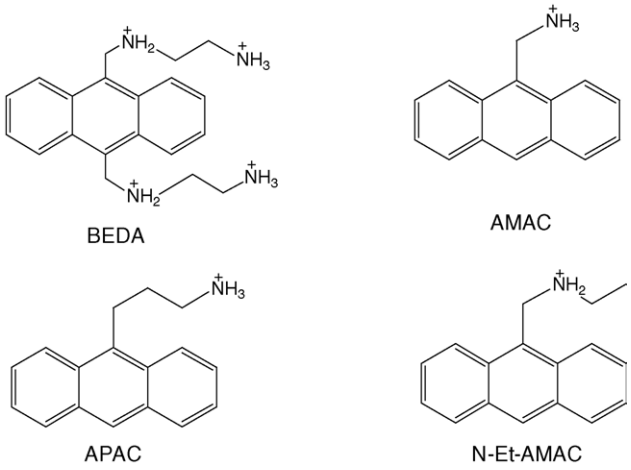

Chart 2. Structures of BEDA, AMAC, APAC, and N-Et-AMAC.

Increasing the ionic strength decreases the phosphate–phosphate repulsion, and this results in the contraction of the helix [14]. Both intercalation and groove binding are expected to decrease with increased ionic strength, but it is unlikely that both binding modes will be decreased to the same extent. This approach may provide a simple method to resolve the two binding modes, and binding of BEDA is investigated as a function of ionic strength. Data are presented here to show that the side chain as well as the ionic strength influence the preferred binding mode of BEDA to a significant extent. According to the Boltzmann distribution, small changes in the relative energies of these states is predicted to have a significant impact on their relative populations. Current data show that it is possible to influence the extents of intercalation and groove binding modes by varying the ionic strength.

Another motivation to study the interaction of BEDA with DNA is related to our long term interest in the encapsulation of biomacromolecules in the galleries of layered metal phosphates [15]. The negatively charged DNA is not expected to interact with the negatively charged metal phosphates, unless the charge on DNA is neutralized or reduced. Binding of the tetra cationic BEDA to DNA is expected to result in significant reduction of negative charge on DNA, and this should encourage binding of DNA to negatively charged surfaces. Current data show moderate binding of BEDA to DNA, enhanced affinity due to electrostatic interactions, and the resolution of the binding modes by the ionic strength studies.

2. Experimental

Calf thymus DNA (CTDNA), type I was purchased from Sigma Chemical Co., and the sample was purified according to published protocols [16]. Stock solutions of DNA were prepared with Tris buffer (5 mM Tris–HCl, 50 mM NaCl, pH 7.2), unless mentioned otherwise, and the concentrations have been expressed in base pairs. All reagents were of analytical grade.

2.1. Synthesis of BEDA

BEDA was synthesized by a modification of the reported procedure [4]. To a solution of 9,10-bisbromomethylanthracene (100 mg, 0.275 mmol, 1 eq.) in tetrahydrofuran (THF, 5 ml), ethylenediamine (0.110 ml, 1.65 mmol, 6 eq., in 5 ml of THF) was added over a period of 1 h, at 0 °C. The reaction mixture was stirred for additional 15 h, and the solvent has been evaporated under reduced pressure to give a viscous liquid. The residue was washed with hexane and then with ethyl ether (3 × 20 ml portions)

to produce a crude yellow product. Recrystallization of the crude product from a mixture of methanol and toluene (1:1) yielded pure product, (40% yield, mp: 185–86 °C), UV–vis: 356, 374, and 430 nm (ε_{394} = 10,200 M^{-1}/cm). Fluorescence: 403 and 423. ^{1}H NMR (ppm, multiplicity, and relative intensity): 8.43, multiplet, 4; 7.76, multiplet, 4; 5.21, broad, 4; 3.52, multiplet, 4; 3.21, multiplet, 4. These data match with those reported in the literature [21].

2.2. Isothermal titration calorimetry

The binding constants with CT DNA were estimated by isothermal titration method using VP-ITC from MicroCal Inc., CT DNA (100 μM, 5 mM Tris, 50 mM NaCl, pH 7.2) solution was loaded into the calorimetric cell (1.4167 ml), while the reference cell contained water, and both cells have been thermally equilibrated at room temperature. BEDA solution (400 μM BEDA, 5 mM Tris, 50 mM NaCl, pH 7.2) was degassed under reduced pressure, loaded into the syringe, and predetermined volumes of the probe solutions were injected into the cell under constant stirring. The number of injections, the volume of each addition as well as the time interval between successive injections were chosen using the software, and the whole process was automated. Heat produced or absorbed due to each addition of the titrant is recorded and the corresponding thermograms have been obtained. The resulting data were analyzed using Origin software (v.5.0, Microcal Inc.) to estimate the binding constant, binding site size, enthalpy of binding, entropy of binding and the free energy of binding. Each experiment was repeated multiple times, each data set were fitted several times with different initial estimates, and statistically significant parameters have been obtained.

2.3. Absorption spectral studies

Absorption spectra were recorded on SLM Aminco 3000 diode array spectrophotometer, which has been interfaced with an IBM personal computer. Concentrations of CTDNA solutions were determined spectrophotometrically by using its molar extinction coefficient (ε_{258nm} = 13,600 M^{-1} cm^{-1}) [17]. Purity of CTDNA sample was checked by monitoring the ratio of the absorbance at 260 nm to that at 280 nm [18]. Absorption titrations with CTDNA were performed by keeping the concentration of the probe constant, while increasing the concentration of CTDNA, and the data have been corrected for small increases in the volume (<10%) during the titration.

2.4. Fluorescence studies

Fluorescence spectra were recorded using an SLM 48000 spectrophotometer interfaced with an IBM personal computer. As in the case of the absorption titrations, a concentrated solution of CTDNA was added to the probe solution. The probe concentration was kept constant while increasing the DNA concentration, and the spectra have been corrected for volume changes. Probe/DNA mixtures were excited at their corresponding isosbestic points, wavelengths where the absorption is independent of DNA concentration, and the isosbestic points have been previously determined from the absorption titrations.

2.5. Binding plots and hypochromism

The spectral changes observed in the absorption titrations were used to calculate the intrinsic binding constant (K_b), using the Scatchard Eq. (1) [19]. In Eq. (1), C_f is the concentration of the free probe, $r = C_b$/[DNA] where C_b is the concentration of the probe bound to DNA, and n is the binding site size. Concentration of the bound probe is given as, $C_b = \Delta A/\Delta\varepsilon$ where $\Delta A = A_f - A_b$ and $\Delta\varepsilon = \varepsilon_f - \varepsilon_b$. A_f and A_b are the absorbances at the corresponding peak positions of the free and bound probes, respectively. The symbols ε_f and ε_b are the extinction coefficients of the free and bound BEDA at the corresponding wavelengths, respectively. Half-reciprocal plots of absorbance versus 1/[DNA] were used to obtain ε_b, and the binding plots have been constructed from these data using Eq. (1).

$$\frac{1}{C_f} = K_b n \left(\frac{1}{r}\right) - K_b \quad (1)$$

2.6. Circular dichroism (CD) studies

The CD spectra were recorded on a JASCO J-710 spectropolarimeter interfaced with a Dell Optiplex personal computer, and the data have been acquired using software from JASCO. Solutions containing the probe and CTDNA (67–300 μM) were placed in a quartz cell (1 cm path length), and the spectra have been recorded in the 300–500 nm region. The operating parameters of 1 nm bandwidth, 10 millidegrees sensitivity, and 4 s response time were used to average upto16 scans, or more, for each sample.

2.7. Helix melting studies

Helix melting studies were carried out by a Cary Win 100 spectrophotometer equipped with a thermostat, which was controlled by a Dell Optiplex personal computer. Helix melting was monitored by following the absorbance of the sample at 280 nm, or at 260 nm, as a function of temperature. The melting temperature (T_m) was determined from the first derivative of a plot of absorption versus T.

2.8. Differential scanning calorimetry (DSC)

The DSC experiments were performed on a Calorimetry Sciences Corporation (CSC) 6100 Nano II differential scanning calorimeter with a cell volume of 0.299 ml, which has been interfaced with a personal computer (Dell Inc.). In a series of DSC scans, both the cells were first loaded with

buffer solution, equilibrated at 10 °C for 10 min and scanned from 10 to 100 °C at a scan rate of 1 °C/min. The buffer versus buffer scan was repeated once and upon cooling, the sample cell was emptied, rinsed and loaded with the DNA solution. Typically, a solution of 68 μM CT-DNA solution in 5 mM Tris 50 mM NaCl buffer (pH 7.2) in the presence or absence of 25 μM BEDA (in the same buffer) were scanned against a buffer solution from 10 to 100 °C at a heating rate of 2 °C/min. The samples and reference solutions were degassed for at least 5 min at room temperature, and they have been carefully loaded into the cells to avoid bubbles. Cells were carefully cleaned before each experiment. A constant pressure of 3 atm was maintained over the solutions to prevent possible degassing of the samples, on heating. A background scan, recorded with the buffer in both the cells, was subtracted from each sample. Reversibilities of the thermal transitions, on these time scales, were checked by examining the calorimetric traces during the second heating cycle.

The excess molar heat capacity of the sample was calculated from the raw data by using the mean molecular mass of 330 g mol^{-1} of nucleotides, and the partial specific volume of the CT DNA equal to 0.73 ml/g. Each value reported here represents the average of at least three experiments, and the melting temperature showed only small deviations (±0.5 °C) between identical samples.

2.9. Photocleavage studies

The supercoiled pUC18 DNA (from Bayou Biolabs) was dissolved in Tris buffer (5 mM Tris–HCl, 50 mM NaCl, pH 7.2). For irradiation, the PTI Model A1010 with a 150 W Xenon-Arc Lamp was used. A monochromator, and WG-345 filter were used to isolate the 374 nm wavelength for irradiation. The eppendorf tubes containing the samples were placed horizontally in the light path for irradiation.

The DNA photo-damage by BEDA was monitored by agarose gel electrophoresis where the conversion of supercoiled pUC18 DNA to nicked circular/linear DNA was monitored. The irradiated samples along with the light and dark controls were loaded onto a 1% agarose gel, and the gel has been run for 70 min by applying 100 V. The buffer used for electrophoresis was TBE (6.055 g Tris Base, 0.2922 g EDTA, and 3.090 g boric acid dissolved in 500 ml water, pH 8). Ethidium bromide was used to stain the gels, the DNA bands were photographed, and the DNA bands were scanned using Adobe Photoshop/NIH Image software. The conversion of supercoiled DNA to the nicked circular form was computed from the relative intensities of the corresponding bands.

3. Results and discussion

By placing appropriate substituents at 9 and 10 positions (Chart 2) of the anthryl probes, their DNA binding properties can be modulated. Placing multiple charges on the side chains of BEDA, for example, is expected to improve the overall binding. Due to its high charge, BEDA is expected to respond sharply to solution conditions [20–25]. Results from calorimetric and spectroscopic investigations show that the preferred binding mode of BEDA can be modulated by ionic strength.

3.1. Isothermal titration calorimetry

Thermodynamic parameters for the association of BEDA with CT DNA were measured directly by isothermal titration calorimetry (Fig. 1A). A concentrated solution of BEDA (400 μM, 5 mM Tris, 50 mM NaCl, pH 7.2, 25 °C) was added in small volumes, over a number of injections to a solution of CT DNA(100 μM, same buffer). Each injection of BEDA solution resulted in release of heat, and the binding saturated toward the end of the titration. In order to account for the contribution of the heat of dilution to the above data,

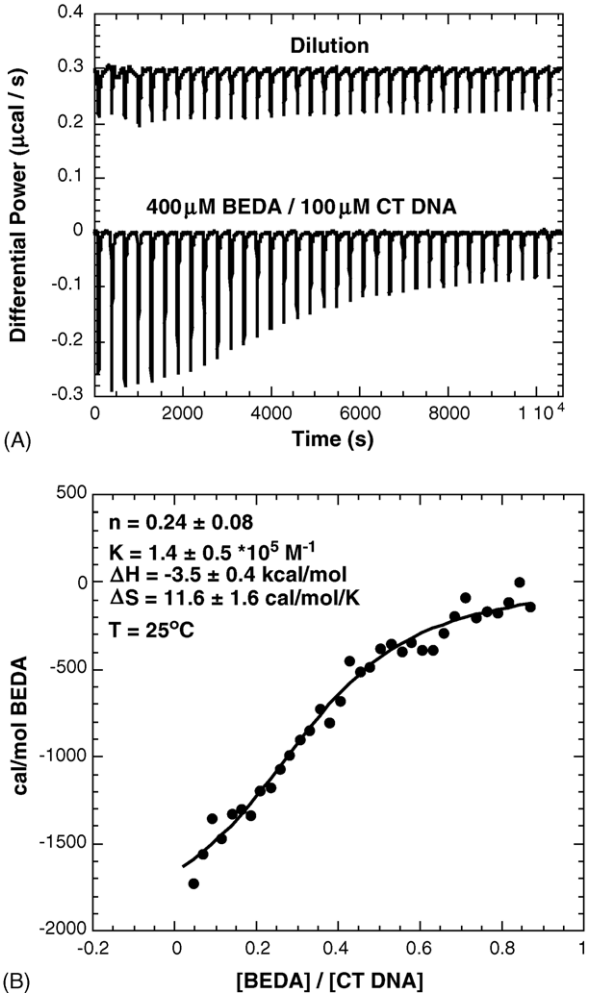

Fig. 1. (A) Raw data of the isothermal calorimetric titration curve obtained when a concentrated solution of BEDA (400 μM) was added to CT DNA (100 μM), in equal intervals. Top curve shows the heat produced when BEDA was added to the buffer, under similar conditions. (B) The integrated thermogram obtained from the data shown in part A. The solid line corresponds to the best fit representing, a single binding site model.

a separate titration was carried out in which a solution of BEDA (400 μM) was added to buffer, under similar conditions. Small, but exothermic heat of dilution was noted (Fig. 1A, top curve). Similarly, the heat of dilution of CT DNA was also measured (data not shown). The area under each peak, in each titration, was integrated, and the heats of dilution of the reagents are subtracted from the observed heat of reaction. The corresponding thermogram is shown in Fig. 1B.

To extract the binding parameters of BEDA from the ITC data, the thermogram shown in Fig. 1B was fitted to a single binding site model, and the thermodynamic parameters have been estimated from the best fit to the observed heat release [26]. The data were analyzed with several different initial guesses, and the resulting fits gave consistent values for these parameters. The analysis resulted in, $K_b = (1.4 \pm 0.5) \times 10^5\ M^{-1}$; $\Delta H = -3.5 \pm 0.4$ kcal/mol; $\Delta S = 11.6 \pm 1.6$ cal/mol K; and a binding site size of ∼4 base pairs ($1/n$). Note that the binding constant is nearly an order of magnitude larger than those of AMAC and APAC, measured under similar ionic strength, and pH conditions [9]. Enhanced affinity of BEDA is primarily due to the contributions of the cationic side chains via electrostatic, hydrophobic and, possibly, H-bonding interactions.

Binding of BEDA to CT DNA resulted in a net release of heat, and similar exothermic binding of a number of probes to DNA was reported earlier [27]. Exothermic binding of BEDA is in contrast to nearly thermo-neutral binding of AMAC/APAC [28] and endothermic binding of Mg(II) to CT DNA [29].

3.2. Absorption spectral studies

The interaction of BEDA with CTDNA was monitored in absorption titrations. The absorption spectra of BEDA (11 μM) were recorded in the presence of increasing concentrations of CTDNA (0–132 μM), shown in Fig. 2A. The spectra were corrected for the small changes in the volume, during the titration. The absorption spectra indicate considerable decrease in the absorption at the peak positions of the free probe, and the hypochromism observed here (70% @394 nm) is comparable to those reported for AMAC or APAC (Table 1) [30].

Absorption spectrum of BEDA/CTDNA also indicated isosbestic points (wavelengths at which the absorbance is independent of DNA concentration) at 380, 384, and 399 nm,

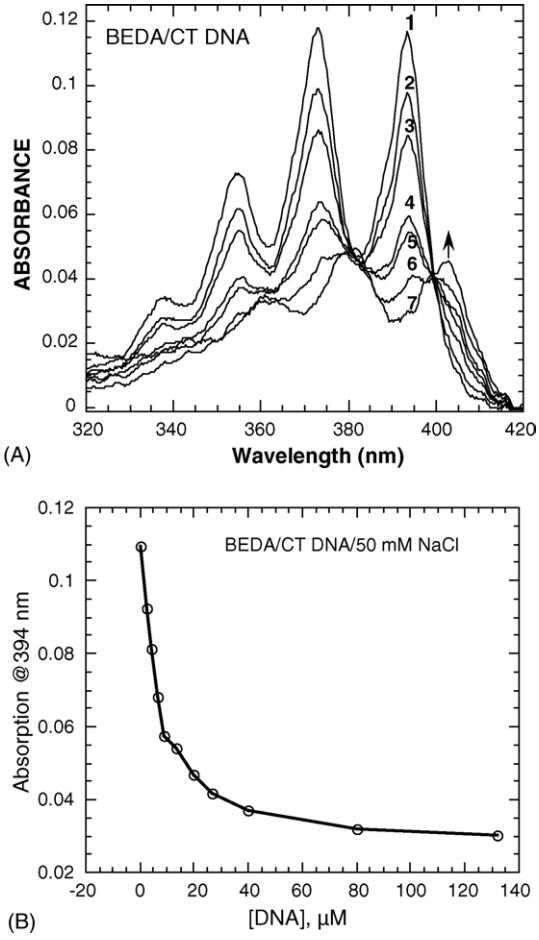

Fig. 2. (A) Absorption spectra of BEDA (11 μM) recorded in the presence of increasing concentrations of CTDNA (0, 2.2, 4.4, 8.8, 13.2, 26.4, and 132 μM). Hypochromism and red shift of the spectra indicate binding of BEDA to CTDNA (50 mM NaCl, 5 mM Tris–HCl, pH 7.2). (B) Plot of absorption of BEDA at 394 nm (free form) as a function of CTDNA concentration. A biphasic decrease in the absorbance at 394 nm is evident in the plot.

and these indicate the conversion of one type of chromophore to another (free and bound) during the titration. The spectra are also red shifted by 9 nm (Table 1), and red shift is the result of a decrease in the energy gap between the highest occupied molecular orbital (HOMO) and the lowest occupied molecular orbital (LUMO, Chart 3). Since binding of the probe to DNA is exoergonic, HOMO of the bound probe is lower in energy than that of the free probe. The observed red shift of the absorption spectrum, therefore, indicates that

Table 1
Peak positions, isosbestic points, percent hypochromism, ε (free and bound) and binding parameters for some anthryl amines (5 mM Tris, 50 mM NaCl, pH 7.2)

Probe	Peak positions (nm)		Extinction coefficient/M^{-1} cm^{-1}; (nm)		Isosbestic points (nm)	Percent hypo-chromism (nm)
	Free probe	Bound probe	Free probe	Bound probe		
BEDA	355, 373, 394	361, 380, 403	10200 (394)	2925 (394)	379, 384, 399	70 (394)
APAC	348, 365, 386	352, 370, 390	7830 (365)	3420 (365)	325, 371, 390	63 (365)
AMAC	348, 365, 385	352, 368, 392	3220 (365)	1276 (365)	362, 367, 388	55 (365)

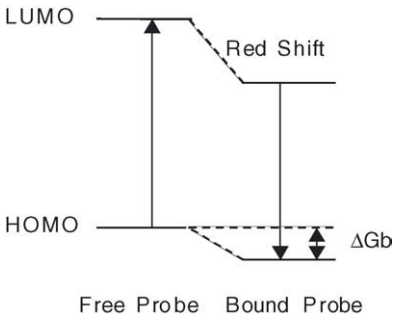

Chart 3. Energy level diagram for the electronic transitions of BEDA.

the first excited state of the probe is stabilized to a greater extent than the ground state.

To check if binding of BEDA to DNA is kinetically slow, the absorption spectra of BEDA/CTDNA were recorded as a function of time. The data indicated that there are no further changes in the absorption spectra, even after four hours (data not shown), and the binding equilibrium was attained rapidly.

To further analyze the nature of the binding interaction, the absorbance of BEDA/CT DNA at 394 nm was plotted as a function of DNA concentration (Fig. 2B). The absorbance decreases rapidly initially, and then more slowly. Such decrease in absorbance indicates the presence of two distinct bound states, and such behavior was not noted with AMAC or APAC. This observation provided a clear handle in resolving the two binding modes.

In an attempt to further clarify the binding modes of BEDA, the influence of ionic strength on the binding was evaluated. Binding of the ligands to DNA is expected to decrease with increased ionic strength [31]. Increased ionic strength screens the phosphate–phosphate repulsion along the helix, and the helix shrinks. Such helix collapse is expected to adversely affect overall binding but it is unlikely that both intercalation and groove binding will be inhibited to the same extent [32]. According to the Boltzmann distribution, small changes in the relative energies of these modes should result in large differences in the relative populations.

Absorption studies were the most revealing, and the absorption spectra of the two bound forms have been distinguished in ionic strength studies. Absorption spectra of BEDA/CTDNA (5 mM Tris, 10 mM NaCl, pH 7.2) recorded at low ionic strength (ratio of concentrations of the probe to DNA is 1:12) are nearly identical to that recorded at 50 mM NaCl. The spectra have been corrected for small changes in the volume, during the titration. The red shift as well as hypochromism are present at low ionic strengths. However, with increase in the NaCl concentration, the absorption spectra of BEDA/CTDNA are blue shifted (375 mM NaCl, otherwise the same conditions), and this shift was also accompanied by a smaller hypochromism (Fig. 3). In control experiments, in the absence of DNA, no such shifts or decreases in the intensities of the absorption peaks of BEDA were detected as a function of ionic strength (Fig. 3).

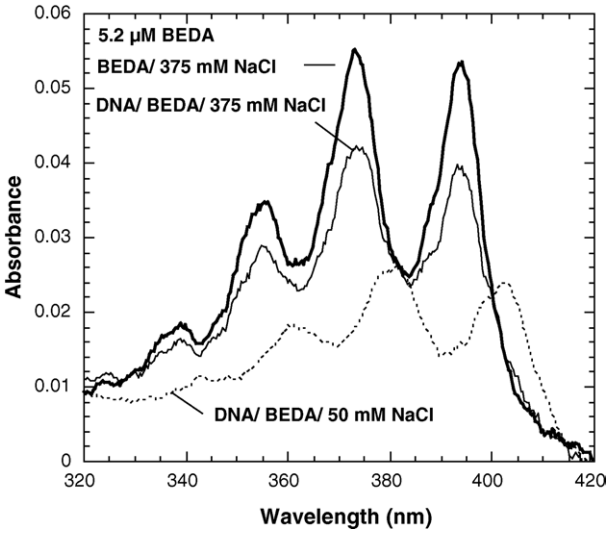

Fig. 3. Absorption spectra of BEDA (5.2 μM)/CTDNA (62 μM) recorded in the presence of increasing concentrations of NaCl (50–375 mM, dotted and thin lines, respectively) in Tris buffer (5 mM Tris, pH 7.2). Data for only two NaCl concentrations are shown. It is clear that at 375 mM NaCl, the absorption peak positions match with those of the free BEDA, but the extinction coefficient of this species is significantly less than that of the free BEDA.

The lack of red shift in the absorption spectrum of BEDA/CT DNA at high ionic strength is most likely due to a new binding mode of the anthrylene probes, not resolved before. One of the two binding modes has a 0–0′ band at 403 nm while the other has a spectrum which is similar to that of the free chromophore, but with lower extinction coefficients. These two modes are resolved by ionic strength studies. Similar un-shifted absorption spectra were also noted when anthryl derivatives with branched substitutions are bound to CT DNA [33], and this was attributed to the groove bound form. In support of this assignment, when a phenyl substituent was placed at the 9 position of the anthracene ring system, intercalation was inhibited, and the corresponding absorption spectrum indicated only a small red shift but significant hypochromism [34]. Current assignment of unshifted, hypochromic spectrum to the groove bound form will be evaluated further.

3.3. Binding plot

The absorbance data are used to construct Scatchard plot (Fig. 4), and the resulting binding parameters are collected in Table 2. The binding plot is linear, and it resulted in a binding constant of $(3.1 \pm 0.1) \times 10^4\ M^{-1}$. The difference between this value and that obtained by the ITC data deserves some comment. Even after considering the large errors in the ITC data (±36%) the binding constants from the two methods are off by a significant value. In the case of the absorption data, the analysis takes into account only the chromophore that is producing the absorption spectral changes, while in the ITC experiment the heat released corresponds to all the binding

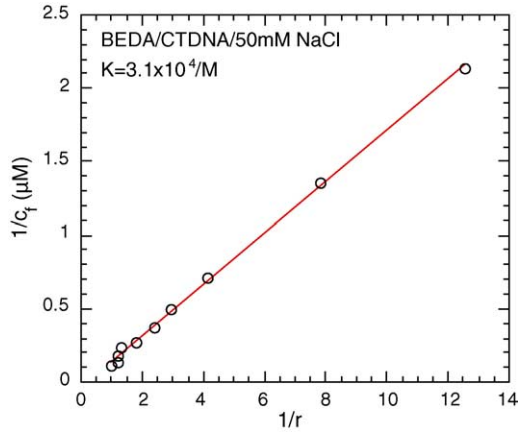

Fig. 4. Scatchard plot for the binding of BEDA (11 μM) to CTDNA (5 mM Tris, 50 mM NaCl, pH 7.2).

events. Still, the binding constant of BEDA is substantially greater than those of AMAC, and APAC, and the enhanced affinity of BEDA is likely due to the increased charge, as well as the interaction of the side chains in the grooves [9].

3.4. Fluorescence studies

Fluorescence spectra provided additional opportunities to examine the details of the interaction of anthryl probes with DNA. The fluorescence spectra of BEDA were recorded in the presence of increasing concentrations of CTDNA (Fig. 5A, 67 μM CTDNA, and 3 μM BEDA, 5 mM Tris, 50 mM NaCl, pH 7.2). The BEDA/DNA samples were excited at the corresponding isosbestic points (379 nm) so that absorbance of the sample is independent of the DNA concentration. The fluorescence spectra indicated red shifts of the peak positions, when compared to the corresponding spectra of the free probe (Table 2). These shifts are consistent with the red shifted absorption spectra and decreased HOMO–LUMO energy gap, at lower salt concentrations. The fluorescence intensities also decreased upon binding to CTDNA (Table 2), and this observation is consistent with the rapid quenching of fluorescence of several anthracene derivatives by CTDNA [9].

Additional evidence for the changes in the binding mode, as a function of ionic strength, was also noted in fluorescence experiments. Addition of a concentrated solution of NaCl to a mixture of the BEDA/DNA (5 mM Tris, 10 mM NaCl, pH = 7.2, probe to DNA ratio of 1:4) resulted in considerable

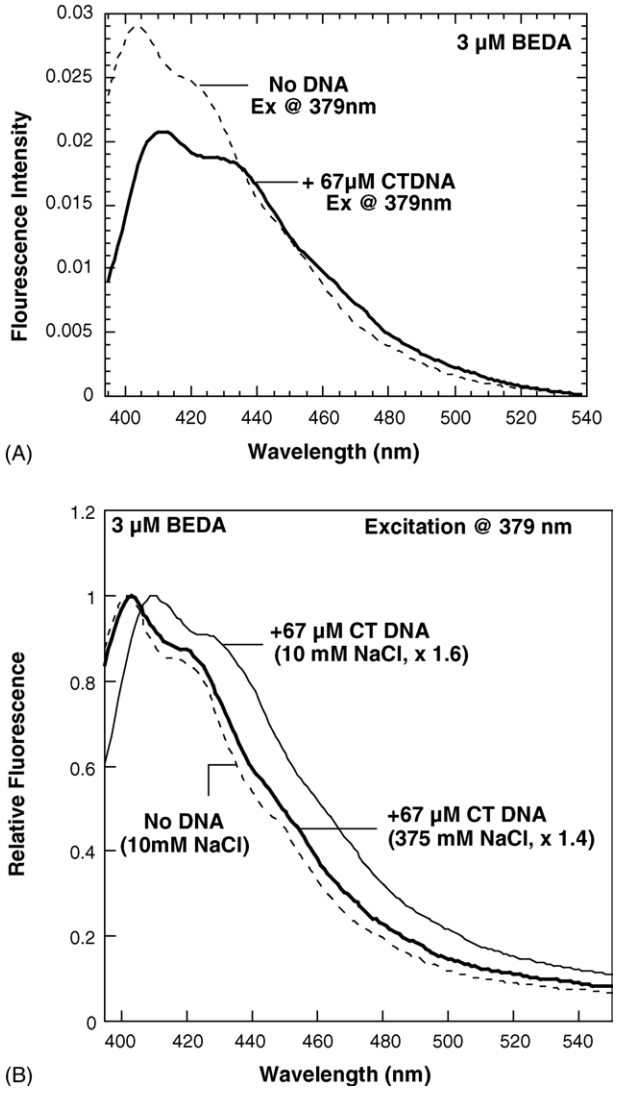

Fig. 5. (A) Fluorescence spectra of BEDA recorded in the absence and presence of CTDNA. (B) Fluorescence spectra of BEDA/CTDNA recorded in the presence of increasing concentrations of NaCl. The spectra are normalized by multiplication with appropriate factors, as marked (concentration needs to be changed).

shifts in the fluorescence maxima, where the peak positions at high ionic strengths matched with those of free BEDA (Fig. 5B). Note that the intensities of the fluorescence spectra of the bound BEDA are less than that of the free, at these high ionic strengths, and these are commensurate with the absorption spectral changes. The absorption as well as the fluorescence spectra of the bound species recorded at high

Table 2
Binding constants, red shifts, and Stokes shifts for anthryl probes bound to CTDNA

Probe	K_b (M^{-1})	Fluorescence, λ_{max} (nm)		Stokes shift (cm^{-1})	
		Free probe	Bound probe	Free probe	Bound probe
BEDA	$(3.1 \pm 0.1) \times 10^4$	403, 423	410, 432	567	610
APAC	$(1.4 \pm 0.1) \times 10^4$	390, 412, 437	391, 413, 438	266	66
AMAC	$(1.5 \pm 0.5) \times 10^4$	392, 412, 438	395, 413, 438	464	194

ionic strength differ from those of the free, and these indicate a distinct binding mode.

3.5. Circular dichroism (CD) studies

Although the anthryl probes shown in Chart 2 are not chiral, their association with the DNA helix is expected to result in strong CD spectra in the 300–400 nm region, away from the DNA absorption bands. Furthermore, induced CD spectra of the intercalated and groove bound chromophores are expected to be different [36]. Intercalation of the anthryl chromophore with its long axis perpendicular to the base pair long axis is expected to give positive CD bands in the 330–420 nm region, and similar spectra are also expected for one type of groove binding where the BEDA side chains are aligned with the minor groove axis. When the ratio of probe to DNA concentration is 1:4, strong, positive, induced CD bands appeared (Fig. 6, 50 mM NaCl, 50 μM BEDA).

Note that the CD peak positions (362, 381, and 404 nm) nearly coincide with those of the absorption peaks of the bound chromophore, 10–50 mM NaCl, but these peaks differ from those of the free chromophore. The CD spectra are assigned to the binding mode with the long wavelength absorption bands, presumably intercalation. However, one intriguing observation was that the CD peak positions are nearly independent of the ionic strength (Fig. 6) and only the intensities decreased. Note that the CD spectra are recorded at high concentrations of the probe (50 μM), and the CD samples showed absorption spectra where the 0–0′ band was broadened, indicating a weak component of the red shifted spectrum. Thus, the multiple binding modes are not readily resolvable by the CD studies.

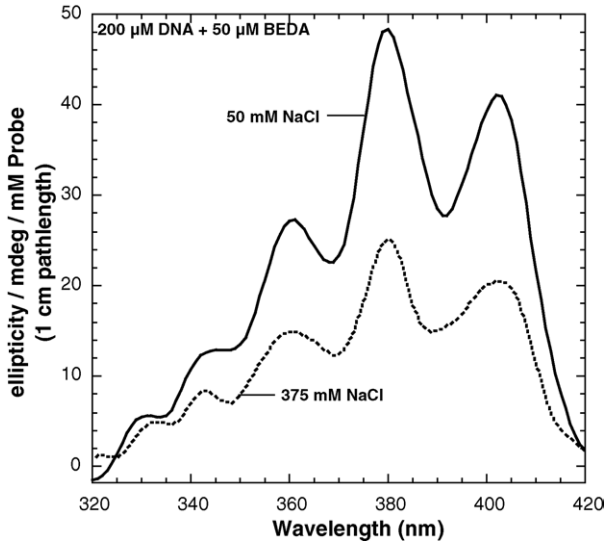

Fig. 6. The induced circular dichroism spectra of BEDA (50 μM) recorded in the presence of CTDNA (200 μM) at 50 and 375 mM NaCl. The decrease in the intensity of the CD bands at high ionic strength is due to overall decrease in the binding of the ligand.

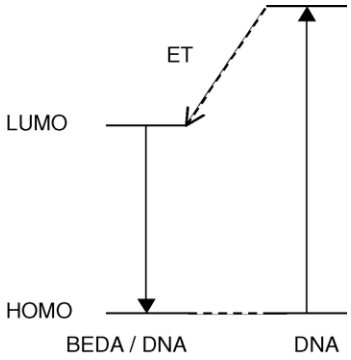

Chart 4. Energy level diagram for the energy transfer from DNA bases to BEDA.

3.6. Energy transfer from the DNA helix to BEDA

Earlier studies reported from this laboratory indicated that excited states of the DNA bases can transfer energy to the anthryl probe, (Chart 4) [35], and energy transfer was most effective when the anthracene derivative was intercalated into the helix at AT sites. Denaturation of the helix, binding of the probe to single stranded DNA, binding to GC sites, or inhibition of intercalation of the anthracene derivative by steric constraints inhibited energy transfer [33]. In the current studies, energy transfer was investigated by recording the excitation spectra and sensitized emission spectra.

Excitation spectra of BEDA/DNA mixtures (265–315 nm excitation, 420 nm monitoring) resulted in intense fluorescence from BEDA/CTDNA (Fig. 7A). The absorption of light in this region by the anthryl chromophore is minimal, while CTDNA has strong absorption bands. Further more, the emission spectrum of CTDNA has a considerable overlap with the absorption spectrum of BEDA, and such overlap favors energy transfer from DNA to BEDA.

The ratio of the excitation spectra recorded in the presence of DNA to that in the absence of DNA is shown in Fig. 7A. This plot accounts for any direct emission from BEDA, and values larger than one indicate sensitization by DNA. A broad, new band at 290 nm with a shoulder at 275 nm appeared in the excitation spectra (5 mM Tris, 50 mM NaCl, pH 7.2). This band is in the region of the absorption spectra of DNA bases, and strongly indicates energy transfer to BEDA. The efficiency of energy transfer, however, is much weaker than that observed with APAC and AMAC [9]. Excitation spectra indicate that intercalation of BEDA is a strong possibility. This conclusion is also consistent with multiple binding modes of BEDA, discussed above.

This interpretation was also supported by excitation spectra of BEDA/CTDNA, recorded in the presence of low and high concentrations of NaCl (Fig. 7B). If the energy is transferred only to the intercalated form, then the observed spectral changes cannot be completely explained. At high ionic strengths, energy transfer to the groove bound state is plausible but weak. This interpretation is consistent with the absorption and fluorescence data.

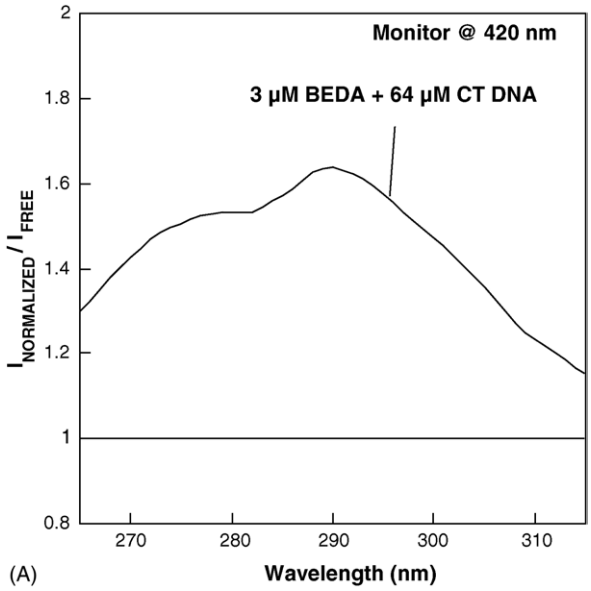

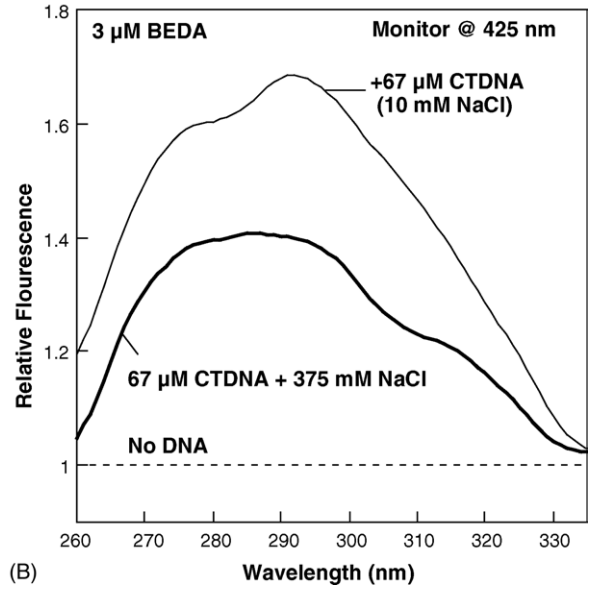

Fig. 7. (A) Excitation spectrum of BEDA recorded in the absence and presence of CTDNA (5 mM Tris, 50 mM NaCl, pH 7.2) while monitoring the emission at 420 nm. The ratio of the intensities is plotted as a function of the excitation wavelength. (B) Excitation spectra of BEDA/CTDNA recorded in the presence of high and low concentrations of NaCl (10, 375 mM). Note that the sensitized emission is weakened at high ionic strength.

Energy transfer from DNA to BEDA was confirmed by recording the sensitized emission spectra (Fig. 8), and note that sensitized emission is more intense than direct emission from BEDA or BEDA/CTDNA (Fig. 5A). The sensitized emission of BEDA/CTDNA is red shifted, when compared to that of BEDA (no DNA), which is consistent with the emission arising from a bound chromophore. Similarly, the fluorescence spectra of BEDA/CTDNA recorded at high ionic strength (375 mM, NaCl, 295 nm excitation, data not shown) indicated weak energy transfer to BEDA. The sensitized fluorescence was still observed at high ionic strength, although, it was considerably weaker.

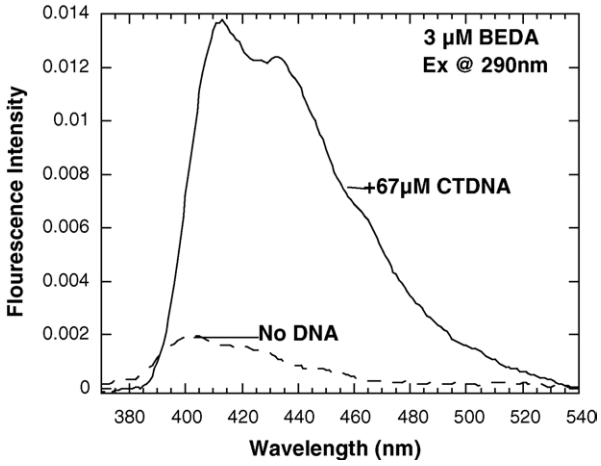

Fig. 8. Sensitized fluorescence spectra of BEDA recorded in the presence of CTDNA (continuous line, 290 nm excitation) while direct emission from BEDA (dashed line) is much weaker, recorded under similar conditions.

3.7. Helix melting studies

Intercalative binding of the anthracene derivatives, often, increases the thermodynamic stability of the helix [36], and enhances the helix melting temperature (T_m). Helix melting was monitored by recording the DNA absorbance at 260 nm, as a function of temperature, and when the double helix dissociates into single stranded DNA, absorbance at 260 nm is increased substantially. The mid point of this transition represents denaturation of the double helix. Binding of many anthryl derivatives improved the helix stability to a large extent, and the helix melting curves of CTDNA with and without BEDA (5 mM Tris, 50 mM NaCl, pH 7.2) are shown in Fig. 9.

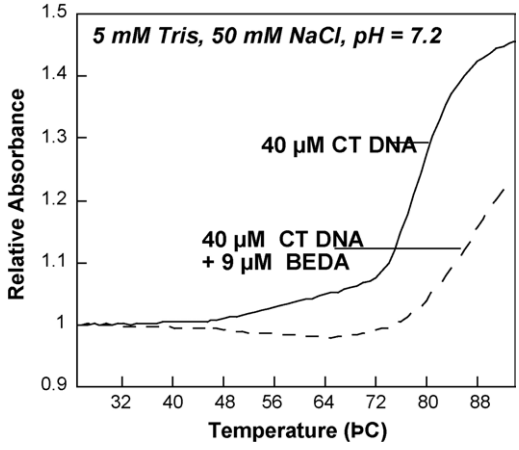

Fig. 9. Helix melting curves of CTDNA recorded in the absence (solid line) and in the presence of BEDA (dashed line). The ratio of absorbance at room temperature to that at higher temperature, measured at 260 nm, was plotted as a function of temperature.

The ratio of absorbance at room temperature to absorbance at elevated temperature is plotted as a function of temperature, and the plots originate at the same *Y*-value, irrespective of their initial absorbance. As the temperature is increased, the ratio remained nearly constant until 72 °C and then began to increase. For example, CTDNA indicated a T_m of 78 °C, in the absence of BEDA, and T_m is increased in the presence of BEDA. The helix melting was not complete even at ~95 °C, and the corresponding value of T_m could not be determined. When intercalation was inhibited by placing large substituents at the 9 and 10 positions of the anthracene probes, the T_m did not increase [37]. Thus, for anthracene derivatives T_m is perhaps a good measure of intercalation.

3.8. Differential scanning calorimetry

The characteristic DSC thermogram of CTDNA is shown in Fig. 10 (solid line). The excess heat capacity plot for a given DNA sequence depends on the base composition [38]. The thermogram of CTDNA is reproducible, and it matched well with the reported profile [39]. The DSC curve showed an endothermic peak centered at 79.5 °C (±0.2) with three "satellite" peaks at higher temperatures. The "satellite" peaks are attributed to highly repetitive, short sequences with higher GC content [40]. The observed transition temperature is in good agreement with the T_m from the melting experiments, presented above. The raw data were converted to heat capacity versus temperature plots, and the enthalpy change was calculated in a model-independent manner (Table 3). The second heating profile of CTDNA, after the first heating and subsequent cooling, did not show any detectable transition, which indicates that the denaturation of CTDNA, is irreversible on these time scales. Due to the high degree of heterogeneity of CTDNA, its renaturation is expected to be quite slow.

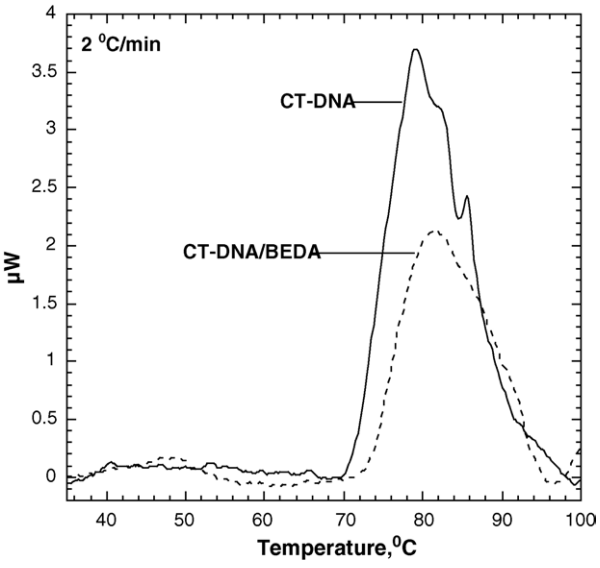

Fig. 10. Differential scanning calorimetry of CTDNA (68 μM, solid line) and a mixture of BEDA (9 μM) and CTDNA (68 μM) (dashed line). Both samples were scanned at a rate of 2 °C/min (5 mM Tris, 50 mM NaCl, pH 7.2).

Table 3
Thermodynamic parameters obtained from the DSC thermograms of CTDNA (68 μM), recorded in the absence and in the presence of BEDA (9 μM)

Sample	T_m (°C)	ΔH (kcal/mol)	ΔS (kcal/K mol)
CT DNA	79.5 ± 0.2	8.5 ± 1	0.025 ± 0.002
CTDNA/BEDA	81.3 ± 0.5	12.5 ± 1	0.035 ± 0.005

The estimated error is the standard deviation of the mean from three separate experiments.

In contrast to the data obtained with CTDNA, the thermogram of BEDA/CTDNA (Fig. 10, dashed line) indicated a smooth transition with the loss of "satellite" peaks but centered at a higher temperature of 81.3 (±0.5) °C. The second heating profile of CTDNA/BEDA did not show any detectable transition, which indicates that the denaturation is irreversible on these time scales. The enthalpy changes, reported here, are model independent, but the entropy changes, are based on the equilibrium model. The transition is not reversible on our time scales, and no permanent changes are expected.

Since only moderate changes are seen in the thermodynamic parameters, ionic strength studies are not undertaken, and in this instance, the spectroscopic measurements are more sensitive than the calorimetric studies.

3.9. Photochemical studies

Encouraged by the interesting DNA binding properties of BEDA, and its reported biological activity, DNA cleavage properties are investigated by using pU18 supercoiled DNA. Irradiation of a mixture of supercoiled pUC18 DNA (20 μM) and BEDA (5 μM) at 374 nm resulted in efficient conversion to the nicked circular DNA (Fig. 11). Some smearing of the lower band is evident, and such smears are assigned to DNA cross-linking. Irradiation of the DNA alone (lane 2) or incubation of the sample in the dark (lane 6) did not result in any detectable conversion to the nicked circular form. Therefore, photoactivation of the ligand is essential for the observed

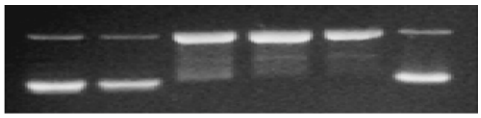

Condition	No BEDA	No BEDA	+BEDA	+BEDA	+BEDA	+BEDA
Lane #	1	2	3	4	5	6
Irradiation time/min	0	60	50	70	90	0
% Supercoiled	88	85	-	-	0	84
% Nicked circular	12	15	>80	>90	100	16
% Linear	0	0	0	0	0	0

Fig. 11. Photocleavage of pUC18 DNA by BEDA (20 μM pUC18 DNA, 2 μM BEDA, 5 mM Tris, 50 mM NaCl, pH 7.2). Samples were irradiated at 374 nm, and stray UV-light was cut off with a WG-345 filter. Efficient conversion of the supercoiled DNA to the nicked circular form is evident from the agarose gel.

conversion. Substantial conversion to the nicked circular form is evident in less than an hour of irradiation (lane 3).

Note that BEDA is much more photoreactive than AMAC [41], and the latter required much longer irradiation times (>2 h) and higher concentrations (50 μM) of AMAC in order to achieve similar conversions. The improved photoreactivity of BEDA over AMAC, and the use of longer wavelengths for the photoactivation are attractive features for the photocleavage applications.

The photochemical conversion of the supercoiled DNA to the nicked circular form was also investigated in ionic strength studies. Briefly, increased ionic strength decreased the overall photocleavage efficiency but this could be due to reduction in the overall binding of BEDA and not necessarily due to the differences in the relative populations of the two binding modes. Further studies are in progress to evaluate the details of this photoreaction.

4. Conclusions

Isothermal titration calorimetry data indicate that BEDA binding to CT DNA is exothermic. The enhanced binding constant, and increased exothermicity, when compared to AMAC/APAC, can be readily assigned to the increased charge on BEDA, and K_b is only moderately greater than the binding constants of the mono-cationic probes, AMAC or APAC and N-Et-AMAC [9]. The charge, therefore, contributes to the binding affinity but not to a very large extent. In addition to ITC, spectroscopic and DSC studies provided further details of binding.

Absorption studies show that binding is accompanied by substantial spectral changes. There are at least two bound forms, one absorbs at 394 nm and another at 403 nm. These assignments are tested in the ionic strength studies. While intercalation was accompanied by substantial red shifts, inhibition of intercalation with large substituents on the anthryl ring did not indicate significant red shifts [33,34]. Therefore, the unshifted, hypochromic spectrum is tentatively assigned to the groove bound form, and this assignment will be tested in future studies. Then, the bathochromic, and hypochromic spectrum will be due to the intercalated form. Since the biphasic behavior is pronounced in the absorption titrations, the spectral data and ITC complement each other. This also explains the differences in the binding constants estimated from these two methods.

The absorption peak positions of BEDA/CTDNA at high NaCl concentration (375 mM) match with those of the free BEDA, but the extinction coefficients of the bound and free forms are substantially different. The ionic strength studies, therefore, resolve the absorption spectra of the two bound states, and these are likely to be the groove bound and intercalated forms. Thus, ionic strength studies show that hypochromic behavior is common to both the bound species, while the red shifts are essentially characteristic of only one of the two. Previous studies showed that when intercalation was inhibited, by placing a bulky substituent at the 9 position of the anthracene ring, the absorption spectra of the bound species are not red shifted. It is entirely likely that the groove binding persists at higher ionic strengths, and the un-shifted spectra correspond to this form of BEDA.

Fluorescence spectral results are consistent with the absorption data, and at higher ionic strengths, the differences between the two bound forms become clear. At higher ionic strengths, the fluorescence intensities are significantly less than that of the free BEDA, which is consistent with the above interpretations. The CD spectra recorded at 1:4 ratio of BEDA to DNA clearly indicated peaks that correspond to the absorption spectra of the bound probe, and the peak positions are independent of the ionic strength. Perhaps, the two binding modes are not readily resolvable in the CD studies.

Excitation spectra show that energy is transferred to BEDA bound to CT DNA, but the transfer is weak, when compared to that observed with AMAC, APAC or N-EtAMAC. At low ionic strength, the excitation band at 280–290 nm is prominent, and as the ionic strength was raised, the intensity of this band has been reduced. This decrease is consistent with the suggestion that intercalative binding mode is inhibited at high ionic strengths. While energy transfer to the intercalated form is facile, energy transfer to the groove bound form cannot be ruled out. Most likely, based on the spectral data as well as the helix melting temperatures, BEDA has significant contribution toward intercalative binding at low ionic strengths and groove binding persists even at high ionic strengths.

The enthalpy and entropy changes associated with the helix to coil transition, observed in the DSC studies, are only minor. Small shift to higher temperature, absence of the satellite peaks, and some asymmetric broadening of the transition are evident. The loss of satellite peaks in the thermogram indicates sequence dependent binding of BEDA, and further studies are needed to test this conclusion. BEDA also exhibited improved photoreactivity when compared to AMAC, and the photoreaction converted the supercoiled DNA to the nicked circular DNA in high conversions, in a short time, and at low loadings. The two binding modes are likely to differ in terms of their photoreactivity, and further studies are planned to evaluate these conclusions.

Acknowledgment

The authors are grateful for financial support from the National Science Foundation (DMR-0300631).

References

[1] S. Neidle, M. Waring (Eds.), Molecular Aspects of Anticancer Drug–DNA Interactions, vols. 1 and 2, CRC, Boca Raton, 1993; M. D'incalci, C. Sessa, Expert Opin. Invest. Drugs 6 (1997) 875.
[2] E. Frei, J.K. Luce, T.L. Loo, Cancer Chemother. Rep., Part 1 55 (1971) 91.

[3] W.L. Wilson, A.J. Weiss, N.C. Andrews, Cancer Chemother. Rep., Part 1 55 (1971) 525.
[4] W.A. Remers, T.P. Wunz, R.T. Dorr, D.S. Alberts, C.L. Tunget, J. Einspahr, S. Milton, J. Med. Chem. 30 (1987) 1313–1321.
[5] R.F. Pittillo, C. Wiilley, Appl. Microbiol. 18 (1969) 519.
[6] W.A. Remers, T.P. Wunz, M.D. Craven, G. Craig Hill, J. Med. Chem. 33 (1990) 1549–1553.
[7] W.A. Remers, R.T. Dorr, D.S. Alberts, B.S. Iyengar, A.M. Solyom, M. Krutzsch, J. Med. Chem. 40 (1997) 3734–3738.
[8] E. Kimura, T. Ikeda, M. Shionoya, Pure Appl. Chem. 69 (1997) 2187;
D.E. Wemmer, P.B. Dervan, Curr. Opin. Struct. Biol. 7 (1997) 355;
J.W. Trauger, E.E. Baird, P.B. Dervan, Nature 382 (1997) 559.
[9] C. Kumar, E.H. Asuncion, W.B. Tan, Tetrahedron 56 (2000) 7027–7040.
[10] W.D. Wilson, F.A. Tanious, R.A. Watson, H.J. Barton, A. Strekowska, D.B. Harden, L. Strekowski, Biochemistry 28 (1989) 1984.
[11] L.S. Lerman, J. Mol. Biol. 3 (1961) 18.
[12] R.H. Terbrueggen, T.W. Johann, J.K. Barton, Inorg. Chem. 37 (1998) 6874.
[13] T.P. Wunz, R.T. Dorr, D.S. Alberts, C.L. Tunget, J. Einspahr, S. Milton, W.A. Remers, J. Med. Chem. 30 (1987) 1313.
[14] B. Lambert, J.-B. LePecq, in: W. Guschlbauer, W. Saenger (Eds.), DNA–Ligand Interactions, From Drugs to Proteins, Plenum, New York, 1986.
[15] A. Chaudhari, C.V. Kumar, Microporous Mesoporous Mater. 77 (2005) 175;
C.V. Kumar, A. Bhambhani, N. Hnatiuk, in: K. Carrado, P. Dutta, S. Auerbach (Eds.), Handbook of Layered Materials, vol. II, Marcel Dekker, New York, 2004.
[16] T. Maniatis, E.F. Fritsch, J. Sambrook, Molecular Cloning: A Laboratory Manual, Cold Spring Harbor Laboratory, New York, p. 458.
[17] B.C. Baguley, E.M. Falkenbaug, Nucleic Acids Res. 5 (1978) 161.
[18] J.K. Barton, J.M. Goldberg, C.V. Kumar, N.J. Turro, J. Am. Chem. Soc. 108 (1986) 2081.
[19] J.D. McGhee, P.H. von Hippel, J. Mol. Biol. 86 (1974) 469.
[20] G.J. Atwell, B.C. Baguley, W.A. Denny, J. Med. Chem. 31 (1988) 774–779.
[21] G.J. Atwell, C.D. Bos, B.C. Baguley, W.A. Denny, J. Med. Chem. 31 (1988) 1048–1052.
[22] B.D. Palmer, G.W. Rewcastle, G.J. Atwell, B.C. Baguley, W.A. Denny, J. Med. Chem. 31 (1988) 707–712.
[23] G.W. Rewcastle, B.C. Baguley, W.A. Denny, J. Med. Chem. 30 (1987) 843–851.
[24] G.J. Atwell, G.W. Rewcastle, B.C. Baguley, W.A. Denny, J. Med. Chem. 30 (1987) 664–669.
[25] G.J. Atwell, B.F. Cain, B.C. Baguley, G.J. Finlay, W.A. Denny, J. Med. Chem. 27 (1984) 1481–1485.
[26] J.B. Chaires, Biopolymers 44 (1997) 201–215.
[27] J. Ren, T.C. Jenkins, J.B. Chaires, Biochemistry 39 (2000) 8439–8447.
[28] Titration of AMAC or APAC into a solution of CT DNA, under similar conditions, did not produce any detectable heat.
[29] A. Chaudhari, J. Thota, C.V. Kumar, Microporous Mesoporous Mater. 75 (2004) 281.
[30] M.J. Waring, J. Mol. Biol. 13 (1965) 269.
[31] C. Cantor, P.R. Schimmel, Biophysical Chemistry, vol. 2, W.H. Freeman, San Francisco, 1980, p. 398.
[32] C. OhUigin, D.J. McConnell, J.M. Kelly, J.M. van der Putten, Nucleic Acids Res. 15 (1987) 7411;
M. Eriksson, H.J. Karlsson, G. Westman, B. Akerman, Nucleic Acids Res. 31 (2003) 6235.
[33] W.B. Tan, Recognition, binding, and cleavage of DNA by anthracene derivatives and heme proteins, Ph.D. Thesis, University of Connecticut, 2000.
[34] H.-C. Becker, B. Norden, J. Am. Chem. Soc. 121 (1999) 11947.
[35] C.V. Kumar, E.H. Asuncion, Chem. Commun. (1992) 470.
[36] C.V. Kumar, E.H. Asuncion, J. Am. Chem. Soc. 115 (1993) 8547.
[37] Placing large substituents at the 9 and 10 positions of the anthryl ring system did not show any increases in Tm while it did not decrease the overall binding affinity (ref. 32, 33).
[38] L. Petraccone, Thermochim. Acta 418 (2004) 47.
[39] H. Klump, in: M.N. Jones (Ed.), Biochemical Thermodynamics, Elsevier, Amsterdam, 1988, p. 100 (Chapter 3).
[40] H. Klump, Ber. Bunsenges Phys. Chem. 91 (1987) 2018;
K.B. Shafit, J. Maio, J. Mol. Biol. 81 (1973) 273.
[41] C.V. Kumar, W.B. Tan, J. Inorg. Biochem. 68 (1997) 177.